Journal for ImmunoTherapy of Cancer

# Exploring markers of immunoresponsiveness in papillary thyroid carcinoma and future treatment strategies

Atish Mohanty ,[1] Michelle Afkhami,[2] Amanda Reyes,[3] Rebecca Pharaon,[3] Holly Yin,[2] Haiqing Li,[4] Dana Do,[3] Diana Bell,[2] Arin Nam,[3] Sue Chang,[2] Thomas Gernon,[5] Robert Kang,[5] Arya Amini,[6] Sagus Sampath,[6] Prakash Kulkarni,[3] Raju Pillai,[2] Vicky Villaflor,[3] Ravi Salgia,[3] Ellie Maghami,[5] Erminia Massarelli[3]

**To cite:** Mohanty A, Afkhami M, Reyes A, *et al*. Exploring markers of immunoresponsiveness in papillary thyroid carcinoma and future treatment strategies. *Journal for ImmunoTherapy of Cancer* 2024;**12**:e008505. doi:10.1136/jitc-2023-008505

► Additional supplemental material is published online only. To view, please visit the journal online (https://doi.org/10.1136/jitc-2023-008505).

Accepted 09 July 2024



For numbered affiliations see end of article.

**Correspondence to**
Dr Erminia Massarelli; emassarelli@coh.org

## ABSTRACT

**Background** The study summarizes the potential use of immunotherapy for *BRAF*-mutated papillary thyroid cancer (PTC) by analyzing the immune profile of City of Hope PTC patient samples and comparing them to the thyroid dataset available in the TCGA database.

**Materials and methods** PTC cases with available formalin-fixed paraffin-embedded archived tumor tissue were identified. RNA was extracted from the tumor tissue and analyzed by NanoString to evaluate their immune gene expression profile. Immunohistochemistry was used to determine the expression of immune suppressive genes and lymphocytic infiltration into the tumor tissue. Thyroid cancer cell lines (MDA-T32, MDA-T68, MDA-T85, and MDA-T120) were used to determine the correlation between the BRAF inhibition and CD274 expression.

**Results** The study found that PTC cases with *BRAF* mutations had higher expression of immune checkpoint markers CD274 and CTLA4, as well as higher tumor-infiltrating lymphocytes, particularly CD4+T cells. Additionally, the study identified immunosuppressive markers expressed by tumor cells like CD73, CD276, and CD200 that could be targeted for immunotherapy. Further experiments using PTC cell lines lead to the conclusion that CD274 expression correlates with *BRAF* activity and that inhibitors of *BRAF* could potentially be used in combination with immunotherapy to treat PTC.

**Conclusions** These findings suggest that PTC cases with *BRAF* mutations or high expression may be correlated with an immune hot signature and could benefit from immunotherapeutic strategies.

### WHAT IS ALREADY KNOWN ON THIS TOPIC

⇒ Papillary thyroid cancer (PTC) is most often successfully treated with surgery and radioactive iodine (RAI), but for the rare cases of metastatic or RAI refractory disease, treatment remains limited to targeted therapy with tyrosine kinase inhibitors given the current efficacy of immunotherapy in this tumor type.

### WHAT THIS STUDY ADDS

⇒ Investigating the correlation between BRAF mutations and the "immune hot signature," which enhances sensitivity to immunotherapy, along with the intricate connection to cell cycle regulation and exploring the novel impact of CD274 expression on immune-mediated cell killing.

### HOW THIS STUDY MIGHT AFFECT RESEARCH, PRACTICE OR POLICY

⇒ From our experiments, we can better identify a subpopulation of PTC patients that may benefit from immunotherapy which can be further refined with future research. Additionally, this research has highlighted new targets in the immune regulatory pathway that could enhance the efficacy of our current treatments.

## INTRODUCTION

Thyroid cancer, which accounts for the majority of endocrine cancer deaths, is one of the most common endocrine malignancies.[1–3] In recent years, the incidence of thyroid cancer has been on the rise due to increased risk factors such as obesity and improved detection techniques.[4] The most common type of thyroid cancer is papillary thyroid cancer (PTC), which accounts for 90% of all cases. Typically, patients with PTC respond well to surgery and radioactive iodine treatment (RAI), but a significant number of patients (about 5%) have distant metastases or become resistant to RAI which makes treatment more challenging.[3] The current standard of care in this setting includes tyrosine kinase inhibitors, namely lenvatinib.[5] Further, various mutations have been identified in the PTC patients which could affect therapeutic response and increase the recurrence rate.

Among these, *BRAF* is the most frequently altered gene, which has been correlated with worse overall survival and lymph node metastasis.[6 7]

The successful development of immune checkpoint inhibitors (ICI) to treat several solid tumors such as melanoma and non-small cell lung cancer (NSCLC) has raised interest in exploring immunotherapy options in thyroid cancers.[8] Programmed death-1 ligand 1orPD-L1 positivity is found to be higher in thyroid cancer than in other forms of cancer, ranging from 23% to 87.5%, likely due to the immune-active state of the thyroid.[9–13] PD-L1 expression has been shown to correlate with lymph node metastases and may potentially be used as a prognostic determinant for more aggressive disease.[13–20]

Although a high PD-1 expression has been reported in thyroid cancer, there is limited understanding of the significance of this association in PTC and its correlation with the *BRAF* V600E mutation. In patients with *BRAF*-mutated melanoma, PD-1 expression increases after combined inhibition of BRAF and MEK signaling.[21] However, the effect of *BRAF* inhibitors on regulating checkpoint markers in PTC cases has yet to be studied. This study aims to investigate the correlation of PD-L1 and other immune checkpoint markers in PTC tumor specimens and to analyze the effect of BRAF inhibition on the expression of these markers in vitro. This research will help to better understand the relationship between PD-L1 expression, *BRAF* $^{V600E}$ mutation, and PTC and potentially inform new treatment strategies for PTC patients.

## RESULTS

### Patient characteristics and treatment history

This pilot study includes a cohort of 19 PTC patients who underwent thyroidectomy or thyroid biopsies at City of Hope Cancer Hospital under the oversight of an Institutional Review Board (IRB 17137). The patients were categorized based on histological features, age, mutational status, metastatic site, and specimen collection stage, as outlined in table 1. 14 patients had a *BRAF* mutation (13 *BRAF* V600E,1 *BRAF* V600R activating mutations), of which 5 also harbored a *TERT* mutation; 2 patients only harbored a *TERT* mutation, and 3 (16%) had neither of the mutations (table 1).

The staging was conducted as per the American Thyroid Association (ATA) and the American Joint Committee on Cancer staging guidelines, which consider age as a high-risk characteristic. Most of the patients (N=13) had lymph node involvement at the time of pathological analysis. Two patients had metastatic disease (one of the patients had bone, lung, and kidney metastasis, whereas the other patient had lung and brain metastasis) while four patients subsequently developed metastatic disease. After the initial surgery, six patients continued to receive targeted therapy (lenvatinib, dabrafenib, entrectinib), and two patients received immunotherapy treatment with pembrolizumab.

### Immune panel profiling by BRAF mutational status

A certified pathologist analyzed H&E-stained slides to differentiate between normal and tumor tissue. RNA extracted from tumor tissue was used to evaluate the expression of genes associated with the immune response using NanoString Technologies' nCounter Pancancer Immune Profiling Panel. The gene expression profile and Z-score values for 21 immune function-associated pathways were analyzed across 19 cases. The results were represented in a heatmap, which displayed the expression levels of these pathways from low to high (figure 1A, online supplemental figure 1 and table 1). To further refine the analysis, the raw counts were normalized to the housekeeping genes, and the differential gene expression of approximately 784 genes between *BRAF*-mutated and *BRAF*-WT PTC cases was evaluated and presented in a volcano plot (figure 1B, online supplemental excelsheet 1). Our analysis revealed significant changes in the expression of several genes between the *BRAF*-mutated and WT cases. A majority of these genes function as modulators of immune response, including CD274 (PD-L1), colony-stimulating factor, B and T lymphocyte-associated protein (BTLA), CCL18, CXCL3, and IL8, (figure 1B). Further, using the ATA guidelines, gene expression comparison was also done between patients with age <55 years (low risk) and ≥55 years (high risk). Interestingly, differential gene expression varied from that of the analysis done between the WT versus mutant, and the lists included interleukins (ILs) and chemokines (figure 1C).

### Analysis of immune cell types by BRAF mutational status

We used the standard cell type markers commonly used in The Cancer Genome Atlas (TCGA) dataset analysis to identify immune cell types within our dataset. Using NanoString's nSolver software, we analyzed the expression of these markers and conducted quality control (QC) assessments across various cell types.

The QC for T cells, macrophages, and CD8-cytotoxic T cells in the dataset was found to be statistically significant (figure 1D, online supplemental figure 2). However, we recorded a broad variability in the distribution of these cell types across samples. Interestingly, we observed unsupervised segregation of samples into groups of low abundance (blue) and high abundance (orange) for various cell types, as depicted in the heatmap (figure 1E). The cell type enrichment scores across samples are presented in online supplemental table 2. Next, we tested the enrichment cell types with respect to *BRAF* mutational status and found higher tumor infiltrating lymphocytes (TILs) in *BRAF*-mutated samples compared with *BRAF*-WT. Treg and CD4 cell types were enriched in the *BRAF*-mutated cases, whereas CD8 and NK56Dim cells were less represented, indicating a potential contribution to an immunosuppressive microenvironment (figure 1F).

**Table 1** Papillary thyroid cancer (PTC) patient specimen analysis (N=19)—characteristics and treatment table

| De-ID | Histology | Age | BRAF status | TERT status | Meta-static disease | Lymph node involvement | Stage at specimen collection | Staging edition | Specimen collection site | First-line treatment* | Additional lines of treatment* |
|---|---|---|---|---|---|---|---|---|---|---|---|
| 54 | Papillary thyroid carcinoma, macrofollicular variant | <55 | Negative | Negative | No | No | PT2N0M0, Stage I | V8 | Thyroid | Surgery (thyroidectomy) | N/A |
| 55 | Papillary thyroid carcinoma, classical | >55 | Positive | Positive | Yes | Yes | pT3bN1bM1, Stage IVC | V8 | Lymph Node | Palliative RT to spine mets; Surgery (thyroidectomy, nephrectomy) | N/A |
| 57 | Recurrent papillary thyroid carcinoma | <55, >45 | Positive | Negative | No | Yes | Recurrent pT4aN1bM0; Stage III | V7 | Larynx | Surgery (thyroidectomy, laryngectomy)+RAI | Sorafenib, lenvatinib, vemurafenib, compassionate use pembrolizumab, palliative RT+cyberknife, encorafenib+ binimetinib |
| 58 | Mult micropapillary carcinomas, classical | <55 | Positive | Negative | No | Yes | pT1aN1aM0, Stage II | V8 | Thyroid | Surgery (thyroidectomy)+RAI | N/A |
| 59 | Papillary thyroid carcinoma | >55 | Positive | Negative | No | No | PT1bN0M0, Stage I | V8 | Thyroid | Surgery (thyroidectomy) | N/A |
| 60 | Metastatic papillary thyroid carcinoma, response to pembro | <55 | Positive | Negative | Yes | Yes | Recurrent pT1bN1aMx, Stage I | V8 | Thyroid | Surgery (thyroidectomy)+RAI | Surgical bed resection+RAI (recurrence), cediranib, lenvatinib, sorafenib, SRS x 5, compassionate use pembrolizumab, dabrafenib+trametinib, palliative RT |
| 61 | Papillary thyroid carcinoma, predominant follicular features | >55 | Negative | Negative | No | No | PT1bN0M0, Stage I | V8 | Thyroid | Surgery (hemithyroidectomy) | N/A |
| 63 | Metastatic papillary thyroid carcinoma; follicular adenoma, lymphocytic thyroiditis | <55 | Positive | Negative | No | Yes | pT3N1bM0; Stage I | V8 | Thyroid | Surgery (thyroidectomy)+RAI | N/A |
| 64 | Metastatic papillary thyroid carcinoma follicular variant; mild lymphocytic thyroiditis | <55 | Positive | Negative | No | No | pT1aN0M0, Stage I | V8 | Thyroid | Surgery (thyroidectomy and neck dissection)+RAI | N/A |
| 65 | Papillary thyroid carcinoma, classical, 6/39 LN positive for carcinoma | <55 | Positive | Negative | No | Yes | PT2N1aM0, Stage I | V8 | Thyroid | Surgery+RAI | N/A |
| 66 | Metastatic thyroid cancer, well-differentiated with follicular architecture. | <55 | Negative | Positive | Yes | Yes | pT3N0M1, Stage II | V8 | Brain | Surgery (thyroidectomy) in 2009; RAI in 2015 and 2016 | Resection+SRS of brain lesions |

Continued

**Table 1** Continued

| De-ID | Histology | Age | BRAF status | TERT status | Meta-static disease | Lymph node involve ment | Stage at specimen collection | Staging edition | Specimen collection site | First-line treatment* | Additional lines of treatment* |
|---|---|---|---|---|---|---|---|---|---|---|---|
| 67 | Anaplastic thyroid carcinoma, arising in association with PTC with focal tall cell features | >55 | Positive | Negative | Yes | Yes | pT2N1a,cM1, Stage IVC | V8 | Central Lymph Node | Surgery+Carbo/ Taxol+Radiation | Lenvatinib |
| 69 | Metastatic papillary thyroid carcinoma, some tall cells | <55, >45 | Positive | Positive | Yes | Yes | pT1bN1bM1, Stage IVC | V7 | Neck Lymph Node | Surgery+RAI | Dabrafenib then lenvatinib |
| 70 | Locally recurrent multifocal PTC involving the paratracheal region & and central compartment, classical type | <55, <45 | Positive | Positive | No | Yes | T3N1bM0, Stage I | V7 | Neck Lymph Node | Surgery+RAI | ChemoXRT with cisplatin |
| 74 | Papillary (classical) thyroid carcinoma | >55 | Positive | Negative | No | PTC is NED | PT1N1bM0, Stage II | V8 | Central lymph node | Surgery | |
| 75 | Papillary thyroid carcinoma, focally invasive into perithyroid soft tissue; lymphocytic thyroiditis and adenomatous nodules; breast cancer | >55 | Negative | Positive | No | No | PT3N0M0, Stage II | V8 | Thyroid | Surgery | |
| 76 | Metastatic papillary thyroid carcinoma | <55, >45 | Positive | Positive | Yes | Yes | PT4aN1bM1, Stage IVc | V7 | Neck Mass | Surgery+RAI | Pembro then lenvatinib then dabrafenib/ trametnib |
| 78 | Papillary thyroid carcinoma, conventional with focal squamous metaplasia | <55 | Positive | Positive | No | No | PT4aN0, Stage I | V8 | Thyroid | Surgery+RAI | |
| 79 | Papillary thyroid carcinoma, follicular variant | >55, >45 | Negative | Negative | Yes | Yes | PT4aN1bM0, Stage IVA | V7 | Neck Lymph Node | Surgery+RAI | Lenvatinib then entrectinib |

*Patients were treated with current first-line SOC at the time of treatment or clinical trial. Subsequent treatments were chosen based on physician/patient preference.
N/A, not available; RAI, radioactive iodine.

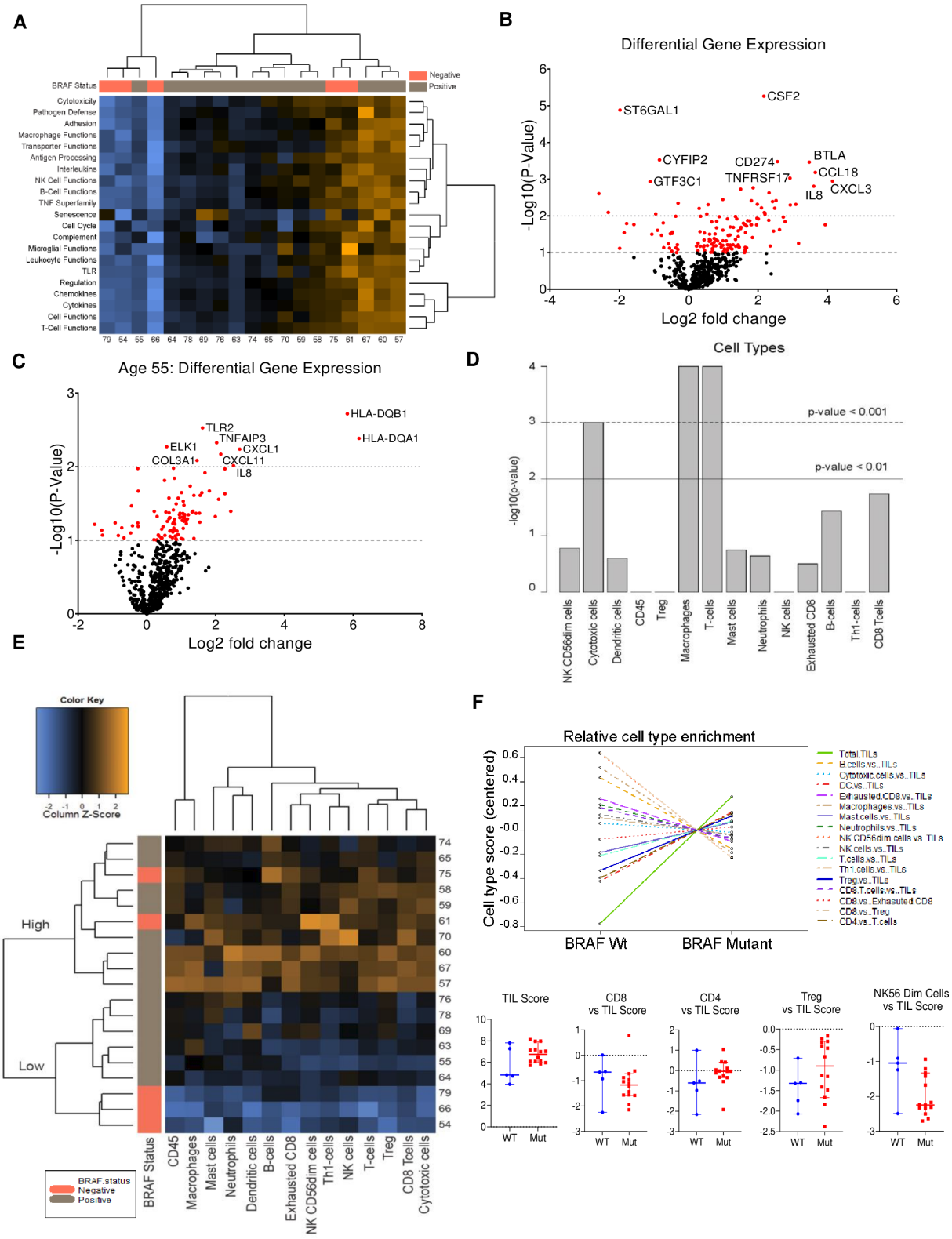


**Figure 1** NanoString analysis of the PTC cases from City of Hope (COH). (A) Heat map representing the enrichment of pathways across *BRAF*-WT and mutated cases. This plot is a high-level overview of pathway scores and also depicts the clustering of samples exhibiting similar score profiles. Orange indicates a high score, and blue indicates low score. (B) Volcano plot representing the differential expression of genes between the *BRAF*-mutated and WT cases. Red dot represents the gene that showed statistically significant changes p<0.01. (C) Volcano plot representing the differential expression of genes between the *BRAF* cases with age <55 and ≥55. The red dot represents the gene that showed statistically significant changes p<0.0. (D) The bar plots represent the cell types that are predicted to be enriched in the PTC tumor tissues. (E) Heat map representing the enrichment of cell types across *BRAF* WT and Mutated cases. (F) CD4 and T-Reg infiltrating TILs are highly enriched in the *BRAF*-mutated PTC compared with *BRAF*-WT. PTC, papillary thyroid cancer; TLC, tumor-infiltrating lymphocyte; WT, wild-type.

### Immune signatures and BRAF mutations in TCGA thyroid cancer dataset

T cells, B cells, and NK cells are the core components of TILs, which contribute to immune activation by recognizing and targeting tumor cells, thereby fostering an antitumor immune response. We focused on analyzing the genes contributing to the T cell function in our cohort and represented them as a heatmap in figure 2. The list of T cell function genes used for the analysis is presented in online supplemental table 3. A set of 12 genes, including CXCL9, CXCL10, CXCL11, CXCR3, CD3, CD4, CD8a, CD8b, CD274, PDCD1, CXCR4, and CCL5, were used to segregate our data set into high (immune hot) and low (immune cold) clusters.[21] However, due to the small sample size, it was not possible to correlate *BRAF* or *TERT* promoter mutations, age, or other risk factors with these groups. Next, we analyzed the expression of the known immunosuppressive markers in our cohort and identified a significant increase in CTLA-4, ICOS, and CD274 expression in the *BRAF*-mutated group compared with the *BRAF*-WT group, as determined by the Mann-Whitney U t-test (figure 2B). Finally, to validate the correlation between the BRAF mutational status and T cell signature, we explored the thyroid cancer TCGA dataset and identified the samples with available *BRAF* mutation status (n=450). The dataset was analyzed, and unsupervised clustering was used to segregate the samples based on the expression of T cell function genes. This analysis revealed three distinct clusters: one exhibiting an immune hot signature (C3), another displaying a cold signature (C1), and a third showing an intermediate signature (C2) (figure 2C). The sum of the T cell function associated gene expression was used to generate a sum score (R's Heatmap package V.2.14.0) which was significantly higher for cluster 3 compared with cluster 1 and 2 (figure 2D). Next, we analyzed the distribution of *BRAF*-WT and mutant samples in these clusters. The analysis confirms a higher percentage of *BRAF* mutants contributing to the clusters exhibiting hot or intermediate signatures compared with the cold cluster(figure 2E). Thus, it can be inferred that patients with *BRAF* mutations are likely to exhibit elevated expression of genes associated with T cell function. This conclusion also suggests that using immunotherapy as a treatment strategy could be advantageous for such thyroid patients.

### Evaluating CD274 and CD73 expression and lymphocytic infiltration in tumor tissue by immunohistochemistry

We performed immune staining on tumor tissue samples from nineteen patients to explore the expression of immunosuppressive and lineage markers genes (CD274, CTLA-4, CD73, CD200, CD20, CD4, CD8, and TTF-1) and determine their correlation with *BRAF* mutation status (online supplemental table 4)[22]. First, the tumor cellularity was measured across the samples, which varies between 50% and 90%, where the majority of the cases had 80% tumor cellularity (table 2).

The Tumor Proportion Score for CD274 across the sample was also quantified and found to be 90% for majority of the cases, irrespective of the *BRAF* mutation status (table 2). We also noticed the higher intensity of the CD274 staining (Grade 2+) in the majority of *BRAF* mutant cases (figure 3A). CD73 expression by immunohistochemistry (IHC) was found to be positive in 14 out of 19 cases and its protein expression correlated with mRNA expression data analyzed through NanoString (online supplemental table 2, figure 3B). We again noticed more robust expression of CD73 in the *BRAF* mutant cases compared with the *BRAF* WT cases. Overall, our data suggested that CD274 and CD73 immunosuppressive proteins were expressed more in the BRAF mutant patients compared with the WT patients, recapitulating the NanoString data.

Next, we employed a multiplex IHC staining technique for detecting CD4+ve T cells, CD8+ve T cells, CD20+ve B cells, and TTF-1+ve tumor cells in tumor tissue. The percentage of lymphocytic infiltration in the tumor was calculated across the samples, and further, the contribution of CD4 and CD8 cells in this infiltration was quantified by the pathologists. The TTF-1 staining was positive for 18 out of 19 cases and was used as a positive control to determine the malignant cells. The lymphocytic infiltration percentage for the mutant samples was significantly higher than the WT samples (figure 3C,D). Further, we analyzed and quantified the staining pattern of tumor-infiltrating CD4+and CD8+ cells. The CD4+cells were significantly higher than the CD8+cells in the mutant tissues, whereas, for the WT, there was no major difference in the cell types (figure 3D). In addition, we also observed CD4 staining positive histocytes in some of the PTC tissues, which may have contributed to the macrophage cell type signature (online supplemental figure 3). Overall, the data were indicative that CD4 cells instead of the CD8 cells were the major contributor to the TIL, confirming the cell type signature obtained from Nanostring analysis.

### CD274 and CD73 expression in PTC cell line models

We used PTC cell lines (T32, T68, T85, and T120) to investigate the relationship between the *BRAF* mutation and its expression on immunosuppressive markers. The T68 cell line had *HRAS* and *TERT* promoter mutations on a *BRAF*-WT background; the T32 cell line had *BRAF* V600E and *TERT* promoter mutations; the T85 cell line had *TERT* promoter, *HRAS* Q61K, and *BRAF* V600E mutations; the T120 cell line possessed a *TERT* promoter mutation, *TP53* R280T, and *BRAF* V600E mutations. High *BRAF* mRNA expression was observed in the T85 and T120 cell lines, and consistent with the BRAF expression pattern, CD274 and CD73 mRNA expressions were also higher in these two mutated cell lines. Likewise, consistent with the *BRAF* low expression, the T68 and T32 cell lines also had low expression for CD274 and CD73 (figure 4A). The mRNA expression pattern for other immune suppressive genes like CD276, ENTPD1, and CD200 did not correlate

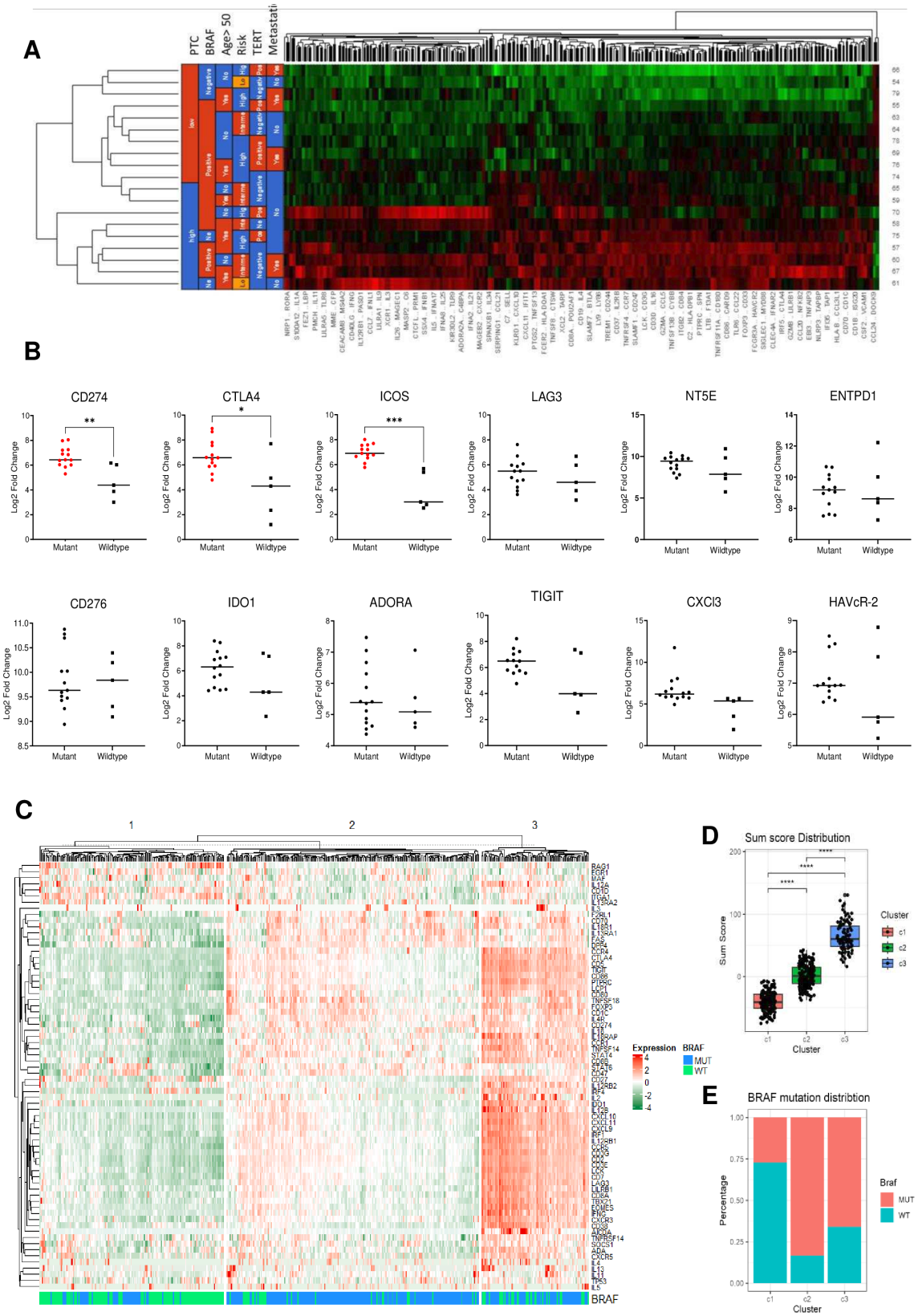


**Figure 2** *BRAF* mutation correlates with immune hot signature. (A) The heatmap represents the expression of all the T cell markers detected in the NanoString data and clustering pattern using *BRAF*-mutated and WT cases. (B) The graph represents differences in the expression of immunosuppressive markers between the *BRAF*-mutated and WT cases. (C) The heatmap represents the expression of all the T cell markers detected in the NanoString data across the TCGA thyroid cohort. (D) The box plot represents the sum of scores for the cold (C1), intermediate (C2), and hot clusters (C3). (E) The stacked bar graph represents the distribution of *BRAF*-mutated cases across all the three clusters. (*p<0.05, **p<0.01, ***p<0.001, ****p<0.0001, ANOVA test). ANOVA, analysis of variance; WT, wild-type.

**Table 2** The table presents the quantification of tumor cellularity, PD-L1 or CD274 TPS (Tumor Proportion Score), intensity, LI (lymphocyte infiltration) percentage, and contributions of CD4 and CD8 lymphocytes in LI

| Sample | Tumor cellularity percentage | TPS- PDL1 percentage | PDL1 intensity | LI percentage | CD4 percentage of LI | CD8 percentage of LI |
|---|---|---|---|---|---|---|
| 54 (Wt) | 80 | 90 | 2+ | <5 | 60 | 40 |
| 61 (Wt) | 90 | <5 | 1+ | <10 | 40 | 60 |
| 66 (Wt) | 80 | 90 | 3+ | <1 | Not quantifiable | Not quantifiable |
| 75 (Wt) | 80 | 90 | 1+ | <5 | 60 | 40 |
| 79 (Wt) | 90 | 90 | 2+ | <1 | 50 | 50 |
| 55 (Mu) | 80 | 90 | 2+ | 15 | 80 | 20 |
| 57 (Mu) | 50 | 5 | 1+ | 40 | 80 | 20 |
| 58 (Mu) | 90 | 90 | 2+ | <10 | <50% | <50% |
| 59 (Mu) | 75 | 90 | 3+ | 25 | 70 | 30 |
| 60 (Mu) | 80 | 90 | 2+ | 15 | 60 | 40 |
| 63 (Mu) | 90 | – | | <5 | 40 | 60 |
| 64 (Mu) | 90 | 90 | 2+ | <5 | 20 | 80 |
| 65 (Mu) | 80 | 90 | 3+ | <5 | 70 | 30 |
| 67 (Mu) | 75 | 90 | 2+ | 20 | 80 | 20 |
| 69 (Mu) | 90 | 90 | 2+ | <10 | 60 | 40 |
| 74 (Mu) | 80 | 90 | 2+ | <5 | 90 | 10 |
| 76 (Mu) | 80 | 60 | 1+ | <10 | 90 | 10 |
| 78 (Mu) | 80 | 90 | 3+ | <5 | 50 | 50 |

with *BRAF* expression (figure 4A). Next, we analyzed the protein expression of these immunosuppressive genes across cell lines. The CD274 and CD73 proteins were highly expressed in the T85 cells, consistent with the mRNA expression. However, for the T32 and T120 cell lines, the protein expression did not mirror the mRNA expression patterns (figure 4B). The combined results of mRNA and protein expression data suggest that *BRAF* mutant samples express CD274, CD73, and CD276, but the degree of the expression varies across samples and appears to be independent of BRAF mutation.

### BRAF knockdown induces CD274 expression in BRAF-mutated PTC cell lines

BRAF is a major component of the MAP kinase signaling pathway (MAPK) and this signaling correlates with CD274 gene expression in lung cancer.[23 24] Likewise, the CD73 (adenosine-mediated) signaling activates PI3K/AKT signaling and also induces CD274 expression.[25 26] Therefore, to test the relationship between BRAF signaling and CD274 or CD73 expression, we transfected the cell lines with *BRAF*-specific siRNA. *BRAF* knockdown reduced mRNA expression of CD274 in two out of three *BRAF*-mutated cell lines (T85 and T120) but caused a 17-fold increase in the T32 cell line. Likewise a twofold increase in expression was observed for the *BRAF*-WT cell line. Unlike CD274, the CD73 mRNA expression consistently decreased across all four cell lines on knocking down *BRAF* (figure 4C). However, the effect of BRAF knockdown on CD274 protein expression was the opposite, resulting in increased expression in T68, T32, and T85 cell lines, but not in T120 cells (figure 4D). Thus, *BRAF* activity has a variable effect on the expression of CD274 at both the transcriptional and translational levels. The overall expression data suggests that *BRAF* signaling could play a significant role in regulating the expression of CD274 in PTC, which is in line with similar observations made in melanoma.[27 28]

### Dabrafenib is superior compared with vemurafenib in regulating PTC cell line growth and inducing cell cycle arrest

We investigated the effect of *BRAF* inhibitors vemurafenib and dabrafenib on the growth of PTC cell lines through live cell imaging (T68 and T85). In the *BRAF*-mutated cell line (T85), the $IC_{50}$ value for dabrafenib was 0.77 µM, whereas for vemurafenib, it was calculated to be 17.3 µM, suggesting a higher potency of dabrafenib compared with vemurafenib (figure 5A,B). Surprisingly, in the *BRAF*-WT (T68) cell line, we found both dabrafenib and vemurafenib inhibited cell growth (IC50 of 2.077 µM, 6.6 µM, respectively) (figure 5C,D). Thus, these results suggest that both drugs can inhibit the growth of *BRAF*-WT PTC cell line, highlighting the need for further investigation into their specificity and alternative targets.

### Dabrafenib-induced cell cycle arrest efficient compared with vemurafenib

We investigated the effect of these inhibitors on cell cycle using Incucyte Cell Cycle assay. The cell lines were treated with vemurafenib or dabrafenib for 72 hours and the

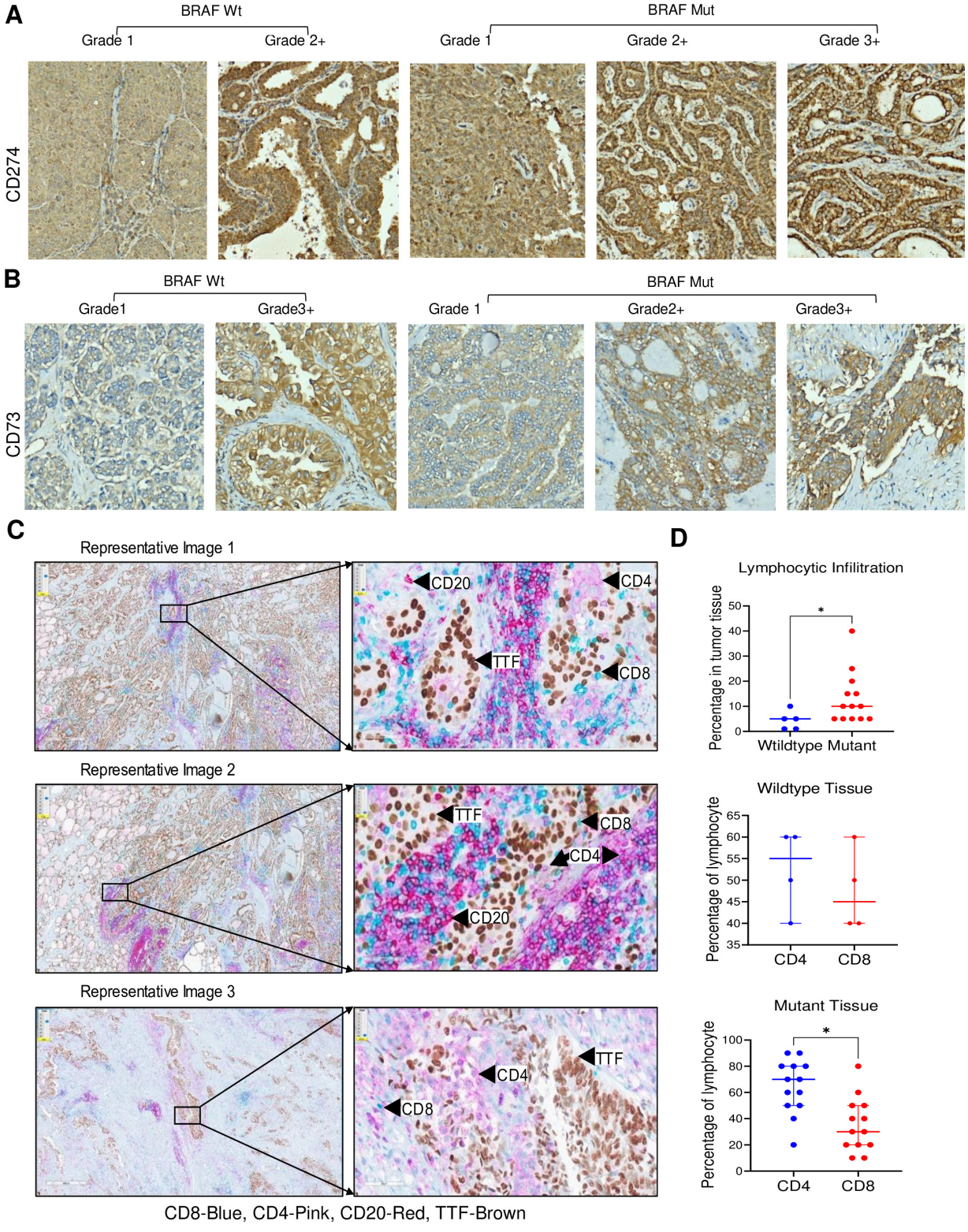


**Figure 3** Expression of immunosuppressive markers correlates to *BRAF* mutation. (A) The tumor tissues of 19 PTC cases were stained with CD274 antibody, and the expression intensity was scored by a COH pathologist. Grade 1 represents the lowest expression, and grade 3+ represents the highest. (B) The tumor tissue was processed to detect CD73, and the expression intensity was scored where grade 1 represents the lowest expression and grade 3+ represents the highest. (C) The images represent the cells positive for cancer cells (TTF-brown), T cells CD8 (blue) and CD4 (pink) in the two representative tumor tissue of *BRAF*-mutated and WT samples. (D) The plot illustrates the percentage of lymphocyte infiltration within the tumor area, as assessed by the pathologist. The lymphocytic infiltration ratio is notably higher for mutant patients (red dots) compared with wild-type patients (blue). Additionally, the percentages of CD4 and CD8 lymphocytes were analyzed. The findings suggest a higher contribution of CD4 lymphocytes compared with CD8, reinforcing the cell type infiltration data. PTC, papillary thyroid cancer; WT, wild-type. * indicates a p value of <0.05

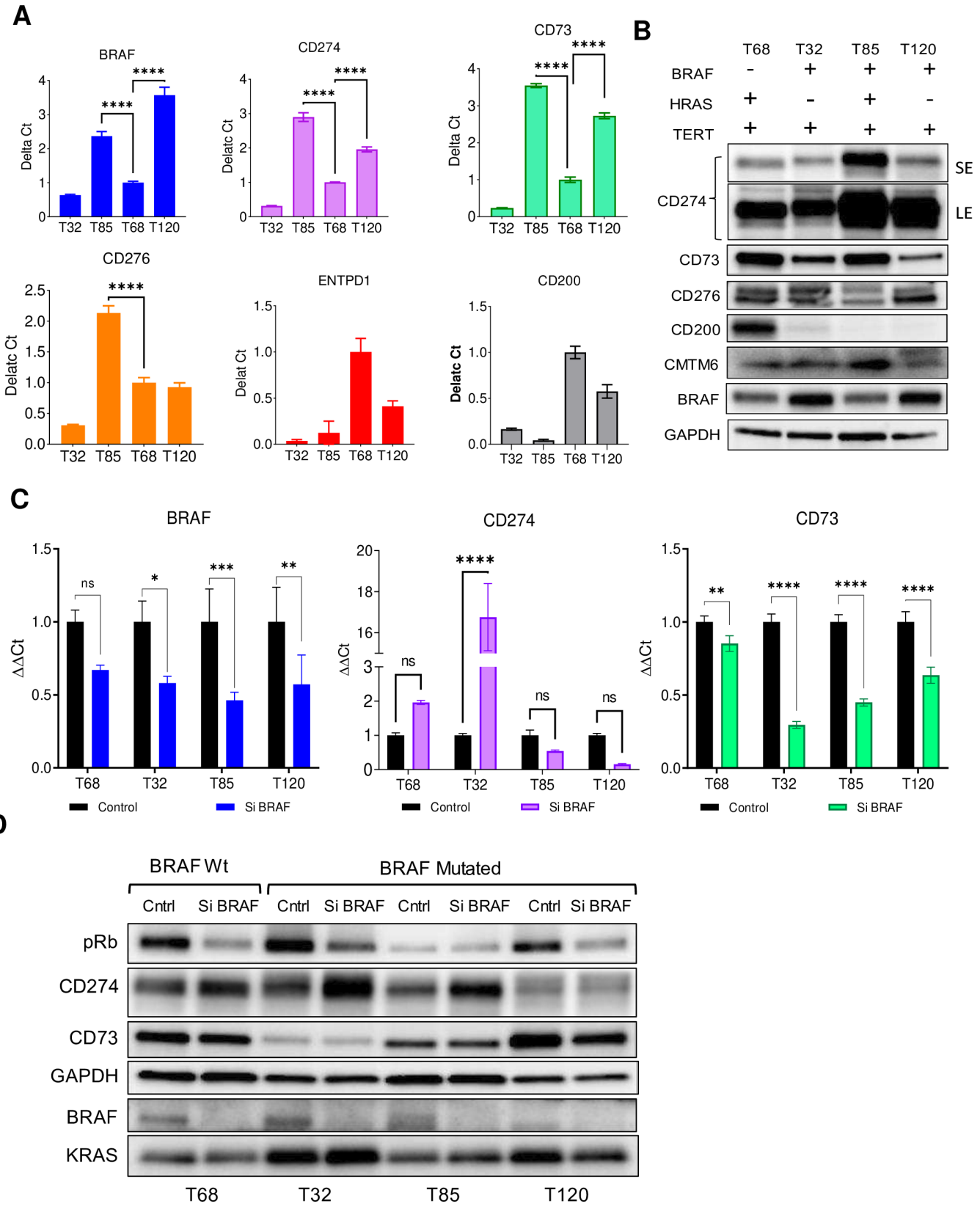


**Figure 4** *BRAF* knockdown induced CD274 expression. (A) The RNA extracted from four PTC cell lines was used to determine the expression of *BRAF*, CD274, CD73, CD200, CD276, ENTPD1, and CD200. The expression in the mutant was compared with the WT cell type. (B) The immunoblot represents the expression of proteins in the *BRAF*-mutated and WT cell lines. (C) The bar graph represents the changes in the mRNA expression of CD274 and other immunosuppressive markers on knocking down *BRAF*. (D) Immunoblot represents the knockdown of *BRAF* and upregulation of CD274 in the *BRAF*-mutated cell lines T32 and T85 (*p<0.05, **p<0.01, ***p<0.001, ****p<0.0001, ANOVA test). ANOVA, analysis of variance; PTC, papillary thyroid cancer; WT, wild-type.

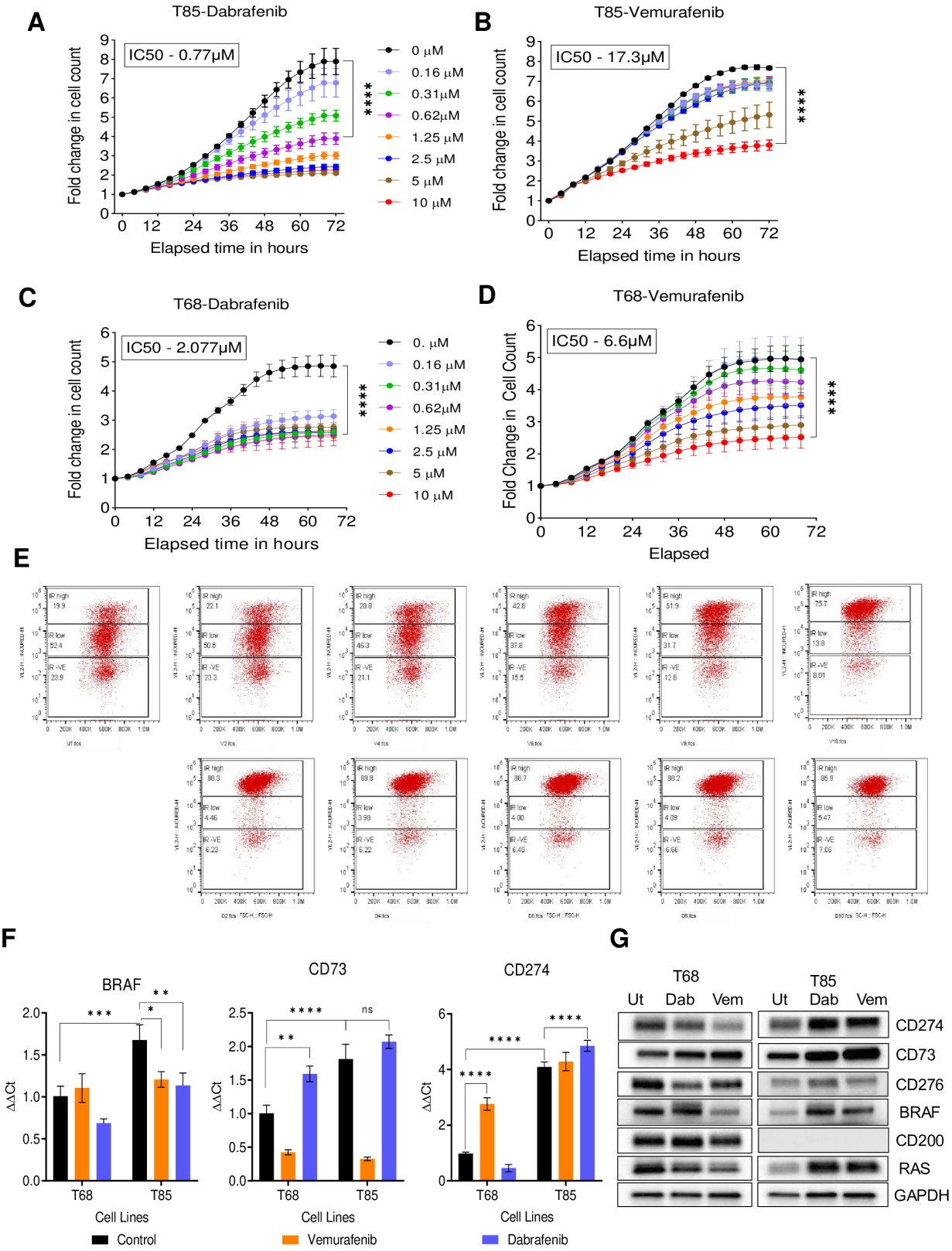


**Figure 5** Cell cycle arrest correlates with CD274 expression. (A, B) The T85 cell line was treated with increasing concentration of *BRAF* inhibitors, and changes in the proliferation were measured using the live cell imaging system. (C, D) Data representing the proliferation changes in the T68 cell lines with respect to *BRAF* inhibitor treatment. (E) FACS data representing the changes in the cell cycle stages of T68 with respect to *BRAF* inhibitors where dabrafenib induced stronger cell cycle arrest. (F) The qPCR data represents the changes in the expression of *BRAF*, CD274 and CD73 in the T68 and T85 cells with respect to the *BRAF* inhibitor treatment. (G) The immunoblot represents the changes in the CD274 and CD73 expression on combining dabrafenib with either binimetinib, temsirolimus, or abemaciclib (*p<0.05, **p<0.01, ***p<0.001, ****p<0.0001, ANOVA test). ANOVA, analysis of variance.

cell cycle changes were analyzed using the Attune NxT Cytometer as mentioned in the 'Materials and methods' section. The cells in G1 phase expressed red fluorescent protein (RFP), G2-M phase expressed green fluorescent protein (GFP), G1 to S transitioning cells exhibited yellow fluorescence, M to G1 transitioning cells had no fluorescence. Interestingly, the G1 phase can be further divided into two subgroups, one with high RFP (20% in untreated cells) and the other with low RFP (50% in untreated cells). This percentage of high RFP cells increased from 22% to 75% with increasing concentration of vemurafenib (10 µM), whereas an 88% increase was observed with 2 µM of dabrafenib (figure 5E). These high RFP represent cells arrested at G1 or cycling slowly, which again suggested dabrafenib to be more effective compared with vemurafenib. Additionally, these data indicate that may be both inhibitors could induce cell cycle arrest through alternative targets.

### Dabrafenib-induced expression of immunosuppressive markers CD73 and CD274

We evaluated the impact of *BRAF* inhibitors on the mRNA and protein expression of *BRAF*, CD274, and CD73 in T68 and T85 cell lines. The cells were treated with vemurafenib or dabrafenib for 72 hours, and the RNA was extracted for quantitative real-time PCR (qPCR) analysis. Dabrafenib inhibited *BRAF* mRNA expression in both cell lines partially (figure 5F, first graph), whereas vemurafenib had no inhibitory effect (figure 5F, first graph). In *BRAF*-mutated T85 cells, a significant change in the CD274 mRNA expression was induced by dabrafenib, whereas for the WT cells, there was no induction (figure 5F, third graph). Consistently, an increase in CD274 protein expression was observed in T85, which correlated with a total increase in RAS protein expression (figure 5G). This suggests that cells induce RAS expression to compensate for BRAF inhibition, and this activation could eventually contribute to increased CD274 expression by activating MAPK signaling.

Dabrafenib also induced CD73 expression in both cell types, whereas vemurafenib downregulated the mRNA expression (figure 5F, second graph). In contrast, dabrafenib and vemurafenib treatment induced CD73 protein expression in both the T68 and T85 cell lines (figure 5G). These results suggest that both BRAF inhibitors cause a significant alteration in the mRNA levels of CD274 and CD73. Moreover, both inhibitors consistently elevate the protein expression of these genes. Additionally, it suggests that either BRAF knockdown or drug-mediated inhibition effectively restrains downstream signaling pathways, consequently halting cell cycle progression and leading to an increase in CD274 and CD73 protein expression.

### Dabrafenib-induced promoter activity upstream of the CD274 transcription start site

In our previous experiments, we observed variability in the expression of CD274 mRNA across the *BRAF* mutant cell lines and also observed differential effect of *BRAF* inhibitors on mRNA expression. To further understand the mechanism of this differential expression, we seek to measure the promoter activity via a luciferase reporter assay using promoter sequences located 1 Kb, 2 Kb, or 3 Kb upstream of the CD274 transcription start site.[29] Likewise, we also used the luciferase reporter assay to determine the mRNA stability assays as shown in (figure 6A, cartoon).[29] The results suggested that the 2 Kb promoter construct of CD274, which contained cis-regulatory elements (a transcription factor binding site), had the highest promoter activity compared with the 1 Kb and 3 Kb constructs (figure 6B). Further, the mRNA stability assay suggests that CD274 mRNA with WT-UTR had faster turnover compared with the mutant UTR in the *BRAF*-mutated T32 cells, which also indicate that changes in the mRNA expression may not be due to stability but due to changes in the promoter activity (figure 6B). Next, we knocked down KRAS or *BRAF* in these cells and determined changes in promoter activity. Interestingly, *BRAF* knockdown increased promoter activity more compared with KRAS knockdown (figure 6C). Further, we determined the effect of dabrafenib on CD274 promoter activity using the *BRAF*-mutated T85 and T32 cell lines. In the absence of any treatment, T85 cells showed significant upregulation of promoter activity compared with T32 cells, which correlated with higher CD274 mRNA expression (figure 6D). However, dabrafenib treatment increased the promoter activity in both the cell lines (figure 6E,F). Thus, the results suggest that *BRAF* inhibitors induce promoter activity upstream of CD274 through epigenetic mechanisms.

### The drug combination effect on CD274 expression

We tested the inhibitory effect of binimetinib (MEK inhibitor), temsirolimus (mTOR inhibitor), and abemaciclib (CDK4/6 inhibitor) on *BRAF*-WT T68 and *BRAF*-mut T85 cell lines and the effect on CD274 and CD73 expression. Binimetinib, temsirolimus, and abemaciclib significantly inhibited the growth of T68 and T85 cell lines with 0.16 µM 0.31 µM and 0.16 µM concentrations of drugs, respectively (figure 7A,B bar graphs). The lowest concentration of these drugs could increase the protein level of CD274 and CD73 in the BRAF-mutated cells, similar to dabrafenib, as shown in the immunoblotting data (figure 7A,B). However, this induction in the CD274 expression was not observed in the BRAF-WT cell line. Furthermore, we assessed the combined impact of binimetinib (0.16 µM), abemaciclib (0.080 µM), or temsirolimus (0.32 µM) with dabrafenib (1 µM) on T85 cells. Following 3 days of drug treatment, the cell viability was quantified using the CCK8 assay. A significant reduction in cell viability was observed with the drug combination of compared with individual drugs, indicating an additive effect (figure 7C–E). Next, we measured the CD274 protein expression through immunoblotting and observed higher expression of CD274 and CD73 in cells treated with the drug combination compared with

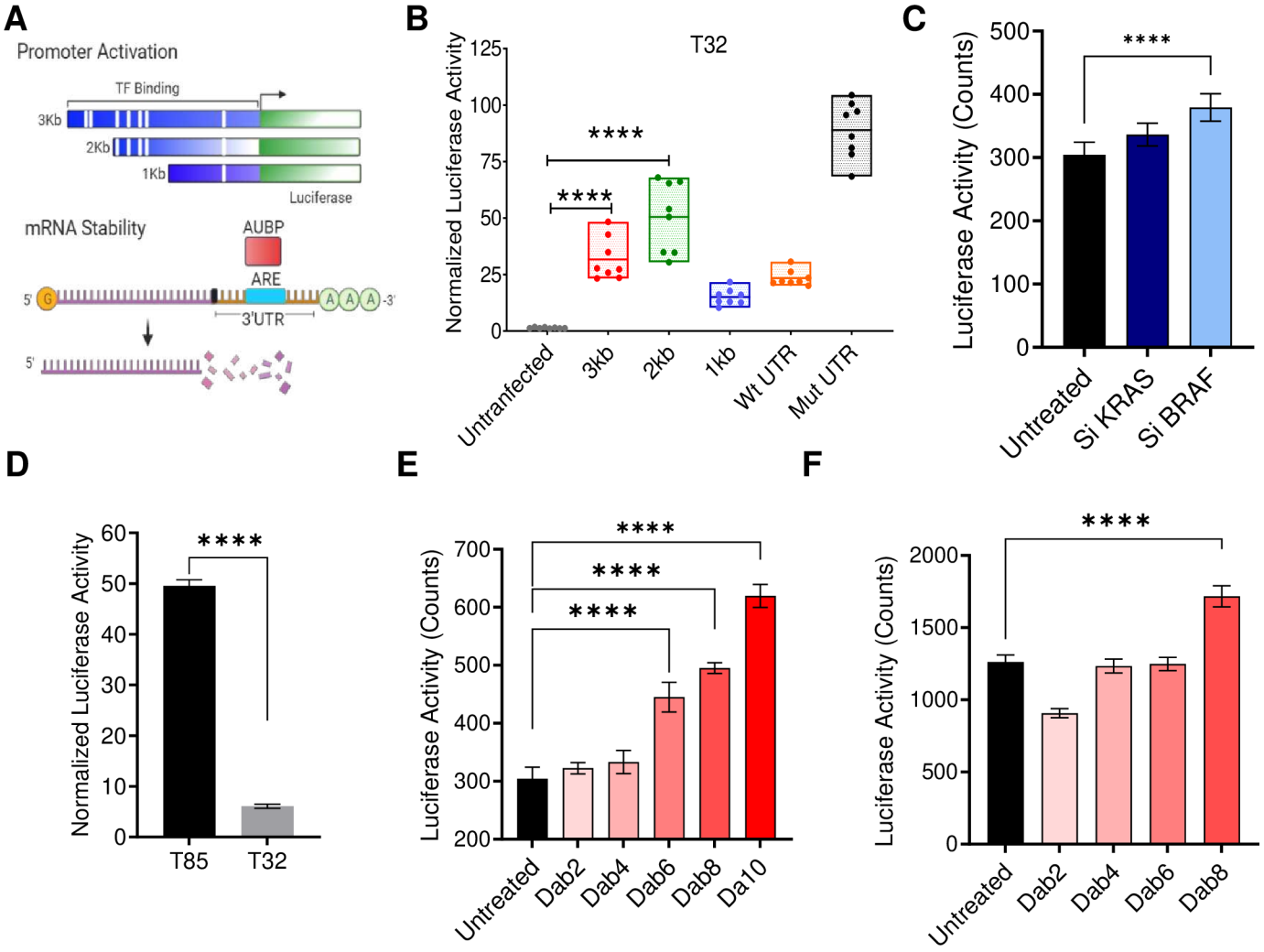


**Figure 6** *BRAF* inhibitor-induced transcriptional changes upstream of CD274. (A) Cartoon showing the design of CD274-promoter-luciferase constructs used for determining the changes in transcriptional activity postdrug treatment. (B) The box plot representing the luciferase activity determined in the cells post 48 hours of transfection, where 2 Kb promoter sequence correlated with maximum activity. (C) Luciferase activity measured in the cells post 48 hours of *BRAF* or KRAS knockdown. (D) The bar graph represents the difference in the promoter activity between the T85 and T32 cell lines. (E, F) Luciferase (Promoter) activity correlated with increased *BRAF* inhibitor concentration in the T68 and T85 cells. (****p<0.0001, ANOVA test). ANOVA, analysis of variance.

individual drugs (figure 7F–H). These findings suggest that combining BRAF inhibitors with MEK, CDK, or mTOR inhibitors could serve as a promising therapeutic strategy for PTC, potentially suppressing proliferation while enhancing the expression of immunosuppressive genes for the utilization of checkpoint inhibitors.

### BRAF-mutated CD274 expressing PTC are prone to CD8-mediated killing

Finally, we explored the significance of CD274 expression on immune cell-mediated cell killing using live imaging assays. The PBMCs were activated using IL-2 and CD3, C28, CD2 activator reagent, and CD8 positive cells were isolated. The T85 and T32 GFP positive cells were co-cultured with the CD8 cells in a ratio of 1/10 or 1/20 and monitored over time. Results indicated a significant reduction in cancer cell growth, even at a low cell-to-immune ratio of 1/10 (figure 8A,B). The endpoint data analysis suggests that the T85 cells that have high CD274 expression were more prone to immune killing compared with T32 cells with lower CD274 expression (figure 8A,B, bar graph).

We analyzed the effectiveness of combining dabrafenib and atezolizumab (atezo) in suppressing the growth of T85 cells. The results showed that co-culturing the T85 cells with CD8, IL-2, and atezo significantly reduced cell growth (figure 8C,D). Furthermore, the addition of dabrafenib to IL-2 and atezo combination significantly enhanced immune cell killing (figure 8C–E). Co-culturing the cell line-derived spheroids with the CD8 cells in the presence of atezo+IL-2 also significantly inhibited the spheroid viability as measured by the reduction in the GFP intensity (figure 8F,G). The immune cell killing became even more effective on adding dabrafenib to the combination of atezo+IL-2 + CD8 (figure 8H).

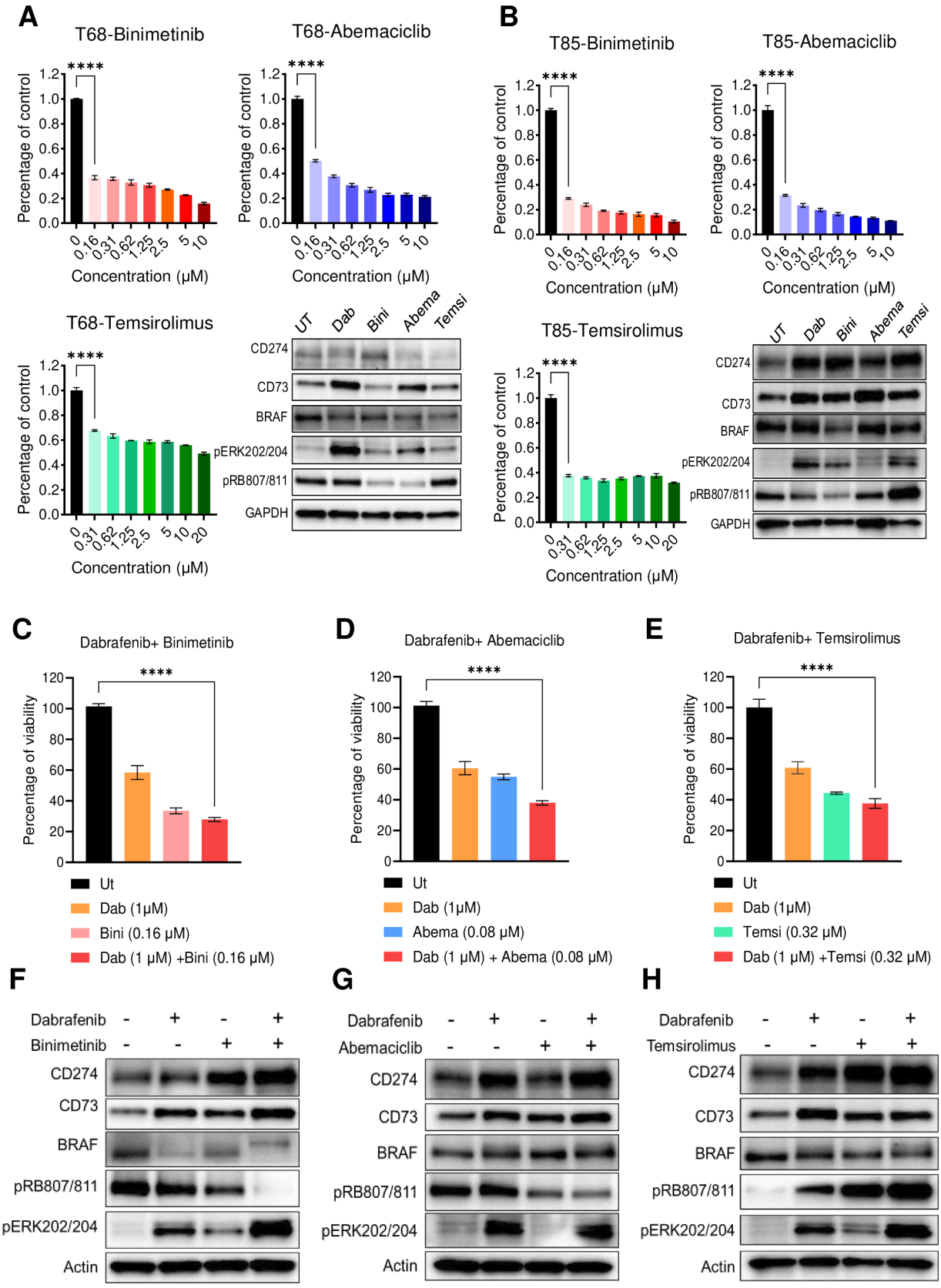


**Figure 7** The drug combination effect on CD274 expression. (A, B) The bar graph represents the percentage change in the growth of T68 or T85 cells on binimetinib, abemaciclib or temsirolimus exposure. The immunoblot shows the change in the expression of CD274 and CD73 on drug treatment. (C) The bar graph represents the effect of drug combinations on the cell viability of T85 cells as measured by CCK8 assay. (D–F) The immunoblot represents the increase in the expression of CD274 and CD73 expression on combining dabrafenib with either binimetinib or temsirolimus, or abemaciclib (*****p<0.0001, ANOVA test). ANOVA, analysis of variance.

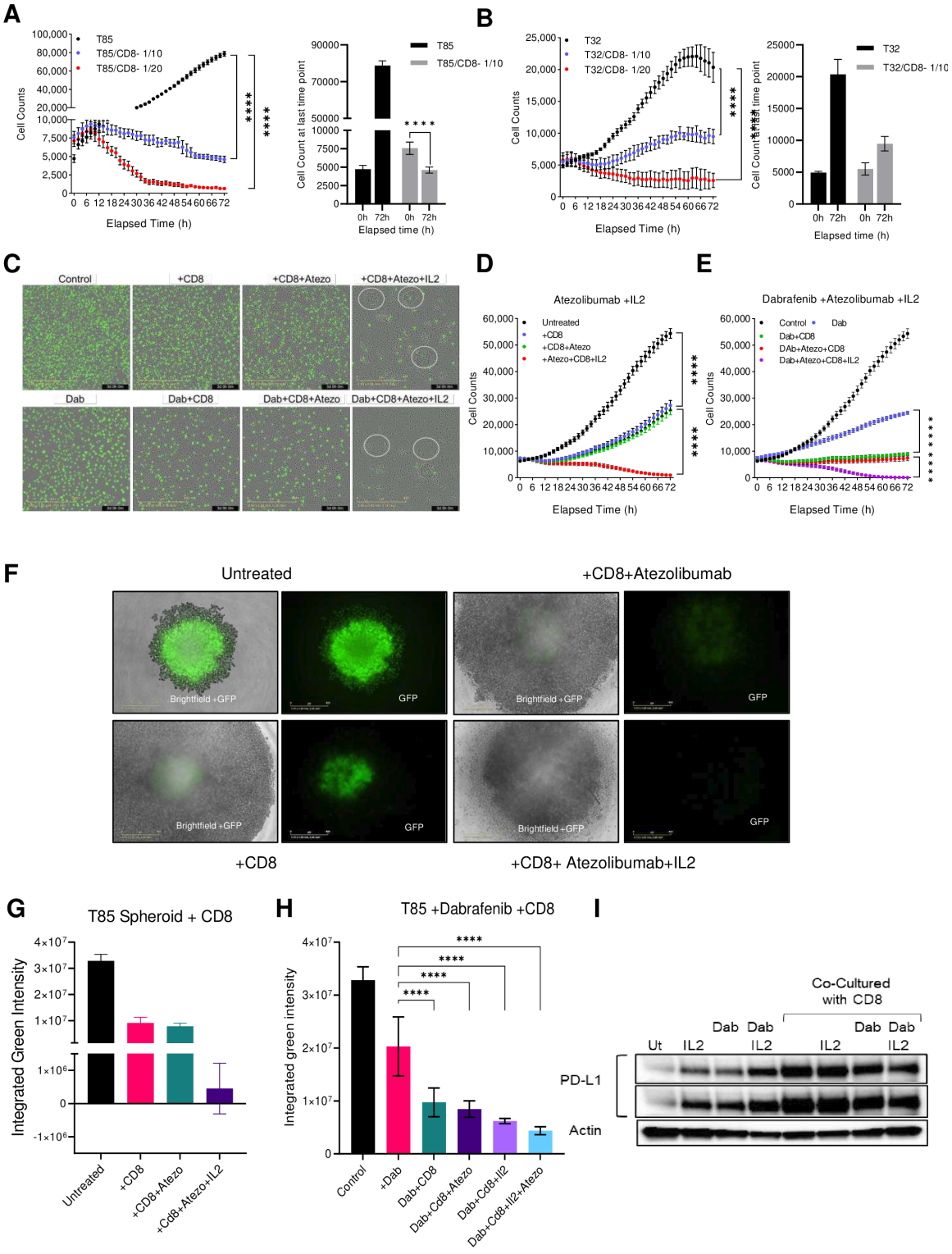


**Figure 8** The synergistic effect of *BRAF* and checkpoint inhibitors in immune cell-mediated killing. (A) The line graph represents the growth kinetics of T85 cells when cultured in combination with activated CD8 cells. The bar graph represents the comparison in growth between monoculture and cocultured T85 cells at 0 and 72 hours time points. (B) The growth kinetics of T32 cells when cultured in combination with activated CD8 cells. (C) The images represent the effect of dabrafenib, CD8, atezolizumab, and IL-2 on the T85 (GFP) cell growth. (D) The growth kinetics of T85 cells when cultured in combination with activated CD8 cells, IL-2, and atezolizumab. (E) The growth kinetics of T85 cells, when cultured in combination with dabrafenib, activated CD8 cells, IL-2 and atezolizumab. (F) The images represent the effect of CD8, atezolizumab, and IL-2 on the T85 (GFP) derived spheroids. Loss of GFP represents a loss of spheroid viability. (G) The bar graph represents the changes in the spheroid viability when cocultured with CD8, IL-2, and atezolizumab. (H) The changes in the spheroid viability when cocultured with dabrafenib, CD8, IL-2, and atezolizumab. (I) The immunoblot represents the changes in the CD274 expression in T85 cells on exposure to IL-2 and dabrafenib n monoculture or coculture. **** indicates P value < 0.001.

Given the potent stimulatory action of IL-2, we explored its effect on the CD274 expression by coculturing the T85 cells with CD8 in the presence or absence of IL-2 and dabrafenib. The addition of IL-2 was found to increase CD274 expression in the T85 cells, which was further induced by the addition of dabrafenib. The CD274 expression was also highly induced by T85 cells when co-cultured with CD8 or with CD8 and IL-2 (figure 8I). These findings suggest that dabrafenib treatment will inhibit cell growth, whereas IL-2 addition will induce CD274 expression, priming the cells for CD8-mediated immune cell killing.

Further, we used the T85 cells expressing the cell cycle markers to determine the effect of CD8 on the cell cycle. The cells were treated with dabrafenib and cultured with and without CD8. The images taken after 24 hours of treatment were presented in figure 9A. The analysis suggests that cells treated with dabrafenib and CD8 have the highest number of red cells, which represents the G1 phase of the cell cycle (figure 9A). Co-culturing with activated CD8 increased the percentage of G1 cells by 39% within 24 hours, whereas dabrafenib increased it by 53%, and the combination dabrafenib and CD8 increased it by 104% (figure 9A, bar graph). Thus, the result suggests that BRAF inhibitors in combination with activated CD8 could have a significant inhibitory effect on cell growth by inducing stronger G1 arrest.

## DISCUSSION

In recent years, ICIs have emerged as an efficacious therapy for advanced cancers but the significance of immunotherapy in the PTC remains controversial. Even though CD274 is expressed in thyroid cancers, ongoing trials with CD274 inhibitors have demonstrated modest results, such as Keynote-158 in which ORR was 3.8% (3/78) in patients with PTC/FTC.[30] The clinical trial results suggested that in association with CD274, other genes or signaling pathways may also contribute to poor response to immunotherapy. Interestingly, this discrepancy is further compounded by the fact that many PTCs have *BRAF* mutations and also express CD274.[31 32] Therefore, we sought to investigate the significance of *BRAF* mutation and its downstream signaling on the expression of immune suppressive markers in PTC tissues. Further, we explore the efficacy of *BRAF* inhibitors in combination with immunotherapy.

The expression analysis of our patient cohort and TCGA data suggested that *BRAF*-mutated PTC cases also higher expressions of other immunosuppressive genes like CD200, CD73, CTLA4, and ICOS. Further, they also exhibited higher infiltration of immune cells (CD4) in the tumor milieu. Altogether, these factors contributed to an 'immune hot signature' that could be used to stratify patients in different risk groups as shown in figure 9B.[33 34] The immune hot group confers sensitivity to immunotherapy and indicates potential benefit from the treatment, as observed in a melanoma case study where a patient in the early 50s, with *BRAF* V600E mutation achieved complete response by adaptive cellular therapy with TILs.[35] In addition to immune hot signatures, tumor mutational burden (TMB) can also be used as a stratification strategy for immune responders as seen in subgroup analysis of Keynote-058, where ORR was 100% (2/2) in the PTC group with TMB-High.[36] Biomarkers like TMB and their correlation with immune hot signatures were also tested in the thyroid cancer dataset of TCGA, and the significance was low compared with BRAF mutation status. Further analysis is needed in the hopes that this information can be used to guide treatment in the future.

The *BRAF*-mutated cases in our study were shown to have higher expression of both CD274 and CD73 compared with the *BRAF*-WT. Previous research established the role of CD73 in activating CD274.[37] Further, there is a correlation between CD73 and the progression of PTC, encouraging further investigation into CD73 as a therapeutic target.[38] A bispecific agent targeting both CD73 and PD-L1 was shown to have promising preclinical data against the Burkitt lymphoma cell line with the potential to move forward as an immunotherapy agent in clinical trials.[39] Our data in combination with previous research suggest immunotherapeutic options against CD73 and CD274 are worth exploring in PTC and should be a subject of upcoming preclinical and clinical trials.

Investigation into the *BRAF* inhibitors dabrafenib and vemurafenib and their effects on cell cycle inhibition demonstrated that both inhibitors were able to induce cell cycle arrest. Dabrafenib had more effective inhibition, which is thought to be related to the fact that dabrafenib is more selective in inhibiting the $BRAF^{V600E}$ as compared with vemurafenib, which can also interact with CRAF.[40] The exact mechanism of their inhibitory effect on *BRAF*-WT is not known, but suggests that by inhibiting NEK9 and CDK16 expression, these inhibitors could potentially slow down the growth of BRAF-WT melanoma cells.[41] From our data, we observed inhibiting *BRAF*-induced KRAS expression, activating both RAS-RAF and PI3K-AKT mediated signaling, which has been known to induce CD274 expression in NSCLC.[26 42–44] Targeting the alternative cell growth pathways has been evaluated previously in *BRAF*-mutated cancers, and the combination of MEK and *BRAF* inhibitors was successful in melanoma, lung cancer, and anaplastic thyroid.[45–47] The inhibition or stimulation of additional agents in the cell growth pathways is a potential avenue for clinically relevant future research.

The significance of CD274 expression in immune cell-mediated killing has yet to be fully explored, and as it is an essential aspect of immunotherapy, this warrants investigation. From our investigation, BRAF-mutated PTC cells with high CD274 expression were more prone to immune mediated cell killing and the immune-mediated cell killing was enhanced on the addition of dabrafenib to immunotherapy. It appears BRAF inhibition sensitizes tumor cells to checkpoint inhibitors, thereby augmenting tumor-killing effects. Combination treatment with BRAF

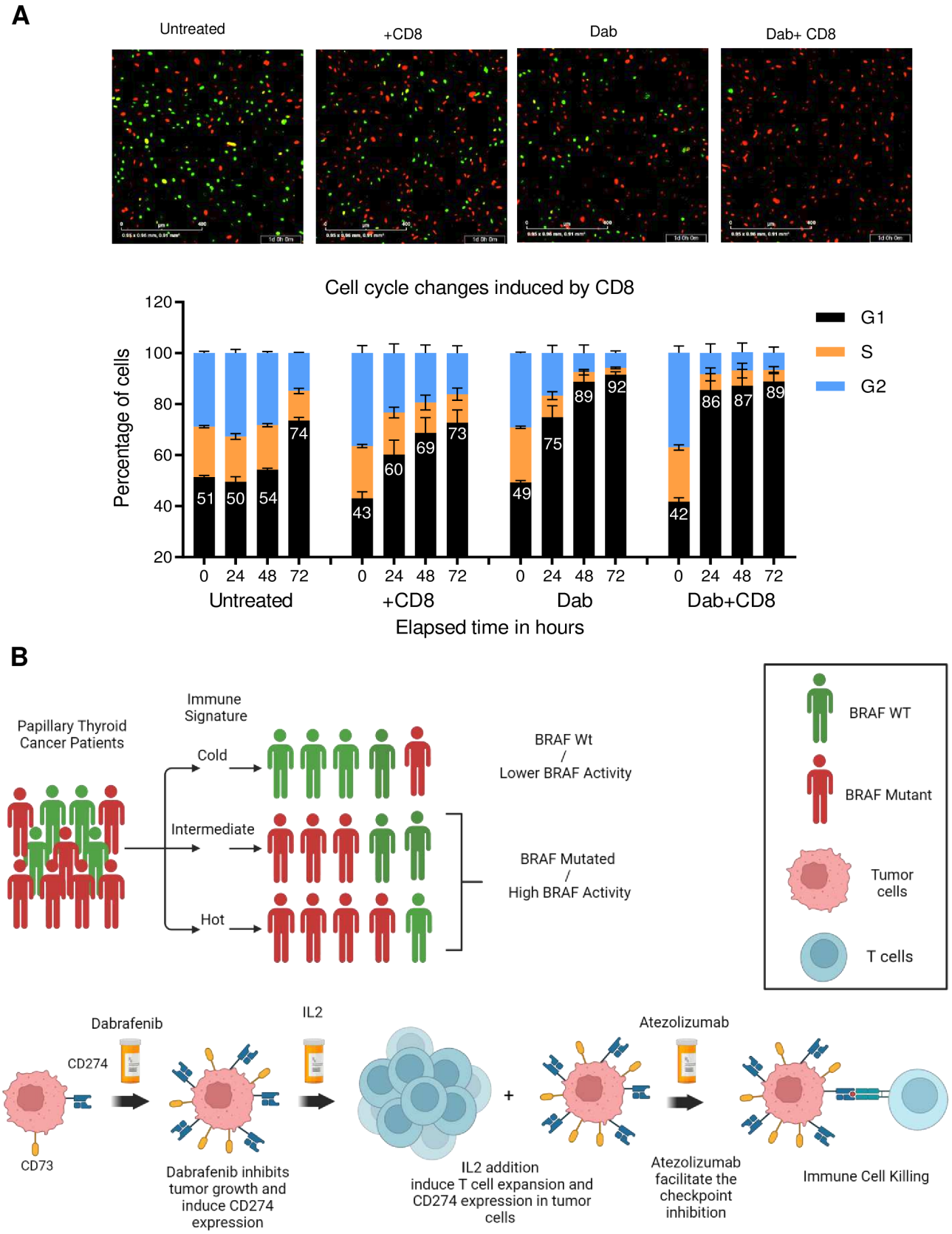


**Figure 9** (A) The images represent the distribution of cell cycle G1 (red), S (yellow), and G2 (green) in the untreated cell or cells treated with dabrafenib and cocultured with CD8. The bar graph represents the cell cycle phase distribution in untreated and treated T85 cells. (****p<0.0001, ANOVA test). (B) The cartoon illustrates the diverse patient population and how patients can be stratified and treated to improve the likelihood of favorable outcomes in those with BRAF mutations exhibiting immune hot signatures. The cartoon schematic presented in the manuscript was created using BioRender. ANOVA, analysis of variance; WT, wild-type.

inhibition and immune check point inhibitors has shown some benefit, especially in large volume of disease or rapid disease progression as seen in previous melanoma studies including the IMspire150 and COMBI-i trials.[48–50] Resistance to this treatment strategy remains a concern and likely contributed to the limited response to immunotherapy after previous BRAK/MEK inhibition in the early Keynote trials and the more recent DREAMseq.[51–53] However, immediate sequential treatment could largely mitigate the opportunity for resistance development, as seen by the success of sequential therapy regimens in the SECOMBIT trial.[54] Therefore, BRAF-mutated papillary thyroid tumor may benefit from similar approaches either with combination therapy or close sequential therapy.

Overall, our data suggest immunotherapy may be a valid therapeutic option in a specific subset of PTC patients, notably patients with tumor characteristics which confer immune sensitivity, but further research is necessary to stratify patients accurately.

## MATERIALS AND METHODS

### Tissue collection and NanoString analysis

This is a retrospective, single-institution cohort study where the inclusion criteria for our study included patients who were seen at City of Hope from 2016 to 2023 diagnosed with thyroid carcinoma with initial papillary histology and pathologic slides available for review. Patients were identified who were diagnosed with papillary thyroid carcinoma, received surgical or systemic treatment at our tertiary care center and had undergone molecular testing on either primary site or metastatic tissue. Additional patients were identified that had tissue at metastatic sites on whom mutational analysis and staining could be performed.

High-risk and low-risk PTC cases (N=19) from 2013 to 2018 with available formalin-fixed paraffin-embedded (FFPE) archived tumor tissue were identified. Several different molecular tests were used on the patient specimen. Most common were iterations of City of Hope's Clinical Molecular Diagnostic Laboratory next-generation sequencing as well as Foundation One, which tests tumor mutations, fusions, and microsatellite instability.

RNA was extracted from the tumor tissue using RNeasy FFPE kit (Qiagen, Hilden, Germany). RNA concentration was determined by the Nanodrop spectrophotometer ND-1000 and Qubit 3.0 Fluorometer (Thermo Scientific, California, USA). It was then analyzed by NanoString to evaluate their immune gene expression profile. The nCounter Systems from NanoString (NanoString Technologies, Washington, USA) was used to quantify gene expression. The Pancancer Human Immune Profiling panel contains 770 genes covering both the innate and adaptive immune system, 40 of which are housekeeping genes. In the Immune Profiling Codeset, there were six positive controls and eight negative controls.

### Cell lines and reagents

Thyroid cancer cell lines (MDA-T32, MDA-T68, MDA-T85, and MDA-T120) were obtained from American Type Culture Collection (Manassas, Virginia, USA). All cell lines were cultured in RPMI 1640 medium (Corning) supplemented with fetal bovine serum (FBS) (10%), L-glutamine (2 mM), penicillin/streptomycin (50 U/mL), sodium pyruvate (1 mM), and sodium bicarbonate (0.075%) at 37°C, 5% CO2.

### Antibodies

Antibodies against *BRAF* (cat #: 14814), CD274 (cat #: 60475), CD276 (cat #:58798), CD73 (cat # 13160), RAS (cat #: 91054), CMTM6 (cat #: 19130), phospho-Rb (S807/811) (cat#:8516), KRAS (cat #: 33197), p-ERK (cat #: 4370) were purchased from Cell Signaling Technology (Danvers, Massachusetts, USA). Cyclin D1 antibody was purchased from Invitrogen (cat #: MA5-14512) (Waltham, Massachusetts, USA). GAPDH (cat #: SC-365062) antibody was purchased from Santacruz Biotechnology, Dallas, Texas, USA.

### Western blotting

Cell were lysed using 1X RIPA buffer, quantified, and denatured in 1X sample buffer at 95°C for 5 min. Protein samples (10 µg) were run on 4%–15% TGX gels (Bio-Rad, Hercules, California, USA) and transferred onto nitrocellulose membranes. Blots were blocked with 5% skim milk in TBS-T and probed with primary antibody diluted in 2.5% BSA in TBS-T overnight at 4°C. After three washes with TBS-T, blots were incubated with HRP-conjugated secondary antibodies for 2 hours at room temperature. After three more washes, bands of interest were visualized via chemiluminescence using WesternBright ECL HRP substrate (Advansta, Menlo Park, California, USA) and imaged with the ChemiDoc MP imager (Bio-Rad,USA).

### Quantitative real-time PCR and RNAseq

qPCR reactions were performed using TaqMan Universal PCR Master Mix (Thermo Fisher Scientific, Waltham, Massachusetts, USA) and analyzed by the Quant Studio7 Real-time PCR system (Life Technologies, Grand Island, New York, USA). Total RNA isolation from cells were performed basing on the manufacturer's protocol RNeasy Plus Mini Kit (Qiagen Cat #: 74134). A 1 µg of RNA was used for cDNA synthesis using the manufacturing protocol from Quanta Bio (Cat#: 101414–106). TaqMan probes for HS03003631-18s, HS00159686-NT5E, HS00204257-CD274, HS00269944-*BRAF*, HS0133302-CD200, HS00969556-ENTPD1, and HS00987207-CD276 were purchased from Thermo Fisher Scientific, Waltham, Massachusetts, USA. The mRNA expression was analyzed using multiplex PCR for the gene of interest and 18s as reference using two independent detection dyes FAM probes and VIC probes, respectively. Relative mRNA expression was normalized to 18s signals and calculated using the delta delta Ct method.

### Bioinformatic analysis of Thyroid Database TCGA

A total of 490 TCGA THCA primary tumor samples RNA-seq data were downloaded from IPA's OmicSoft land Explorer (QIAGEN, https://digitalinsights.qiagen.com/IPA) 37) TCGA_B38 database. Out of 490, 298 samples are BRAF-mutated samples, and the rest are BRAF wild-type samples. The gene expression is measured as FPKM. RNA-seq data are standardized and normalized using z-score normalization. Based on the 70 T cell-related genes, THCA samples were clustered into three distinct clusters using Euclidean distance method from R's Heatmap Pacakge V.2.14.0.[55] Tumor mutation burden (TMB) data were generated from R's UCSCXenaShiny Package V.2.0.0.[56] The boxplot for T cell marker genes score distribution and TMB distribution and the barplot for the Mutation cases distribution are generated using R's ggplot2 package V.3.4.0.[57]

### SiRNA transfection and knockdown experiments

Small interfering RNA against *BRAF* was purchased from OriGene Technologies (Rockville, Maryland, USA) (Cat #: SR319499). JetPRIME transfection reagent (Polyplus Transfection, Illkirch, France) was used to transfect the 10 nM siRNAs according to the manufacturer's protocol [58]. The siRNA sequence use for the transfection is as follows: SR319499B: rGrArGrArUrGrArUrCrArArArCrUrUrArUrArUrAeGrArUrArUTG.

### Immunohistochemistry

Multiplex IHC staining for TTF, CD4, CD8 and CD20 was performed on Ventana Discovery Ultra (Ventana Medical Systems, Roche Diagnostics, Indianapolis, USA) automated IHC stainer. Tissue samples were sectioned at a thickness of 5 µm and mounted on positively charged glass slides. The tissues were deparaffinized, rehydrated, peroxidase activity inhibited and processed for antigen retrieval. Then, the antibodies TTF1: clone#: 8G7G3/1, CD4: clone#: SP35, CD8: clone#: SP57, CD20: clone#: L26 were sequentially added, and heat inactivated to prevent antibody cross-reactivity between the same species. Following each primary antibody incubation, DISCOVERY anti-mouse HQ or DISCOVERY anti-Rabbit NP and DISCOVERY anti-HQ-HRP or anti-NP-AP secondary antibodies were incubated. The stains were then visualized with DISCOVERY ChromoMap, Red, Teal and Purple Kits, respectively, counterstained with hematoxylin (Ventana), and cover slipped. The slides were scanned using the Motic Easy Scanner, and images were used for western.

### Cell proliferation and CCK8 assay

Cell proliferation assays were performed using cell lines T85 and T68. These cells were stably transfected with NucLight Green Lentivirus (# 4624, Essen Bioscience) to accurately visualize and count the nucleus of a single cell. Cells were seeded on a 96-well plate. After 24 hours, vemurafenib or dabrafenib was added at indicated concentrations, and cell growth was monitored every 4 hours. Fold change in cell count was calculated for 72 hours, and IC50 concentration was calculated. For CCK8 cells were seeded at a density of 5000 cells per well in 96 well plates (Cyto One, Cat #: CC7682-7596, Ocala, Florida, USA). Following overnight incubation, the drugs were added to get the desired concentration as mentioned in the results and then incubated for 72 hours. Cell viability was measured using CCK-8 assay, which is based on the principle of bioreduction of WST-8 to soluble formazan dye by live cells (Dojindo, Cat #: CK04, Rockville, Maryland, USA). Absorbance was recorded at 450 nm using a spectrophotometer (Tecan SPARK 10M, Hombrechtikon, Switzerland). The percentage change in viability was determined compared with the untreated cells, and ordinary one-way analysis of variance was used for getting the statistical significance.

### Cell cycle analysis

We used IncuCyte Cell Cycle Green/Red Lentivirus to infect T68 and T85 cells to generate a stable cell line following the manufacturer's protocol (IncuCyte Cell Cycle Red/Green Lentivirus #4779). The stable cell line expressed various fluorescent markers based on their cell cycle phase. The stable cell line expressing red fluorescence represents G1, green fluorescence in S/G2/M and yellow cells are in transition from G1 to S while nonfluorescent cells are moving from M to G1. The stable cell lines were treated with *BRAF* inhibitors, and the cell cycle state was determined after 72 hours.[57] Cells were trypsinized and resuspended (5 million) in PBS with 2% FBS. Cells were stained with Propidium Iodide Ready Flow Reagent (1 drop/1 million cells) (Invitrogen) for 5 min at 4°C. FACS analysis was performed to determine shifts in cell population using the Attune NxT Flow Cytometer (Invitrogen) and FloJo software V.10.

### Luciferase assay

The pGL3 plasmids harboring the 1 kb, 2 kb or 3 kb region of the CD274 promoter were purchased from Addgene (# 107002, #107003 and #107004). Likewise, the pGL3 plasmid harboring the WT or mutant UTR region of the CD274 gene were purchased from Addgene (#107009, #107010). The first assay was to determine the promoter activity using a luciferase reporter assay with promoter sequences of 1 Kb, 2 Kb, or 3 Kb upstream of the CD274 transcription start site. The second experiment was to investigate the mRNA stability of CD274 mRNA by using a reporter assay with 3'-Wt or mutant UTR of CD274 . The principle behind this assay is that mRNA half-life is shorter for the Wt because of the faster turnover compared with the mutant.[28] Each of these plasmids were transfected to the cell lines, and changes in the luciferase activity were determined using the Twinlite Firefly and Renili Luciferase Assay (#6066706, PerkinElmer California, USA).

### Immune cell killing

The healthy human PBMCs were purchased from STEMCELL Technologies, Cambridge, USA (Cat#70025.1).

The immunoCult-XF T cell expansion media (# 10981), CD3/CD28/CD2 T Cell Activator (#10970) and Human Recombinant IL-2 (# 78036) were purchased from STEMCELL Technologie, Cambridge, USA. The PMCS were thawed and cultured according to the manufacturers protocol. The culture was supplemented with fresh media on days 3, 5, 7 and finally the live cells were harvested on day 10. These live cells were used for the immune cell killing assay. The T85 cells that have been used for the cell proliferation assay was used for the immune cell killing assays. The minimum cancer cell to immune cell ratio was optimized, and then the experiment was performed in combination with *BRAF* and checkpoint inhibitors.

**Author affiliations**
[1]City of Hope Comprehensive Cancer Center, Monrovia, California, USA
[2]Department of Pathology, City of Hope National Medical Center, Duarte, California, USA
[3]Department of Medical Oncology and Therapeutics Research, City of Hope National Medical Center, Duarte, California, USA
[4]Computational & Quantitative Medicine, Beckman Research Institute, City of Hope National Medical Center, Duarte, California, USA
[5]Department of Surgery, City of Hope National Medical Center, Duarte, California, USA
[6]Department of Radiation Oncology, City of Hope National Medical Center, Duarte, California, USA

**Acknowledgements** We acknowledge the patients for their consent to use the tumor tissue for the study.

**Contributors** AM and MF: conceptualization, experimentation, analysis, figure preparation, manuscript writing. AR, RPharaon, HY, HL, DD and AN: experimentation, analysis, reviewing, and manuscript writing. SC, DB, TG, SS, RK, AA and RPillai: tissue IHC, tissue resection, clinical information, and pathological analysis. PK, VV, RS, EMaghami and EMassarelli: manuscript writing, editing, reviewing, and analysis. RS, EMaghami and EMassarelli: guarantor, conceptualization, analysis, manuscript writing and editing, project coordinating and funding. The AI was used for refining the sentences and grammatical error corrections.

**Funding** The project was funded with City of Hope Excellence award, with the award number "Excellence Project 2009957". This work has also been partially funded by a philanthropy grant from Deepak Chopra.

**Competing interests** No, there are no competing interests.

**Patient consent for publication** Consent obtained directly from patient(s).

**Ethics approval** This study involves human participants and was approved by City of Hope Institutional Board, IRB-17137. Participants gave informed consent to participate in the study before taking part.

**Provenance and peer review** Not commissioned; externally peer reviewed.

**Data availability statement** All data relevant to the study are included in the article or uploaded as online supplemental information. Not Aapplicable.



**ORCID iD**
Atish Mohanty http://orcid.org/0000-0003-1464-3165

## REFERENCES

1 Siegel RL, Miller KD, Jemal A. Cancer statistics, 2020. *CA A Cancer J Clinicians* 2020;70:7–30.
2 Chen AY, Jemal A, Ward EM. Increasing incidence of differentiated thyroid cancer in the united states, 1988–2005. *Cancer* 2009;115:3801–7.
3 Noone A, Howlader N, Krapcho M, *et al*. SEER Cancer Statistics Review. National Cancer Institute, 1975–2015. Available: https://seer.cancer.gov/csr/1975_2015/
4 Han JM, Kim TY, Jeon MJ, *et al*. n.d. Obesity is a risk factor for thyroid cancer in a large, ultrasonographically screened population. *Eur J Endocrinol*168:879–86.
5 Schlumberger M, Tahara M, Wirth LJ, *et al*. Lenvatinib versus placebo in radioiodine-refractory thyroid cancer. *N Engl J Med* 2015;372:621–30.
6 Elisei R, Ugolini C, Viola D, *et al*. BRAFV600E mutation and outcome of patients with papillary thyroid carcinoma: a 15-year median follow-up study. *J Clin Endocrinol Metab* 2008;93:3943–9.
7 Kim SK, Lee JH, Woo J, *et al*. BRAF V600E mutation: differential impact on central lymph node metastasis by tumor size in papillary thyroid carcinoma. *Head Neck* 2016;38.
8 Ohaegbulam KC, Assal A, Lazar-Molnar E, *et al*. Human cancer immunotherapy with antibodies to the PD-1 and PD-L1 pathway. *Trends Mol Med* 2015;21:24–33.
9 Cunha LL, Marcello MA, Morari EC, *et al*. n.d. Differentiated thyroid carcinomas may elude the immune system by B7H1 upregulation. *Endocr Relat Cancer*20:103–10.
10 Angell TE, Lechner MG, Jang JK, *et al*. BRAF V600E in papillary thyroid carcinoma is associated with increased programmed death ligand 1 expression and suppressive immune cell infiltration. *Thyroid* 2014;24:1385–93.
11 Wu H, Sun Y, Ye H, *et al*. Anaplastic thyroid cancer: outcome and the mutation/expression profiles of potential targets. *Pathol Oncol Res* 2015;21:695–701.
12 French JD, Haugen BR. Thyroid-specific T cells in patients with differentiated thyroid cancer: implications for immune-based therapies? *J Clin Endocrinol Metab* 2017;102:2131–2.
13 Ahn S, Kim TH, Kim SW, *et al*. n.d. Comprehensive screening for PD-L1 expression in thyroid cancer. *Endocr Relat Cancer*24:97–106.
14 Phillips T, Simmons P, Inzunza HD, *et al*. Development of an automated PD-L1 immunohistochemistry (IHC) assay for non-small cell lung cancer. *Appl Immunohistochem Mol Morphol* 2015;23:541–9.
15 Chowdhury S, Veyhl J, Jessa F, *et al*. Programmed death-ligand 1 overexpression is a prognostic marker for aggressive papillary thyroid cancer and its variants. *Oncotarget* 2016;7:32318–28.
16 Severson JJ, Serracino HS, Mateescu V, *et al*. PD-1+tim-3+ CD8+ T lymphocytes display varied degrees of functional exhaustion in patients with regionally metastatic differentiated thyroid cancer. *Cancer Immunol Res* 2015;3:620–30.
17 Bai Y, Niu D, Huang X, *et al*. PD-L1 and PD-1 expression are correlated with distinctive clinicopathological features in papillary thyroid carcinoma. *Diagn Pathol* 2017;12:72.
18 An HJ, Ko GH, Lee J-H, *et al*. Programmed death-ligand 1 expression and its correlation with lymph node metastasis in papillary thyroid carcinoma. *J Pathol Transl Med* 2018;52:9–13.
19 Rosenbaum MW, Gigliotti BJ, Pai SI, *et al*. PD-L1 and IDO1 are expressed in poorly differentiated thyroid carcinoma. *Endocr Pathol* 2018;29:59–67.
20 Xu B, Ghossein R. Genomic landscape of poorly differentiated and anaplastic thyroid carcinoma. *Endocr Pathol* 2016;27:205–12.
21 Sanlorenzo M, Vujic I, Floris A, *et al*. BRAF and MEK inhibitors increase PD-1-positive melanoma cells leading to a potential lymphocyte-independent synergism with anti–PD-1 antibody. *Clin Cancer Res* 2018;24:3377–85.
22 Wang H, Li S, Wang Q, *et al*. Tumor immunological phenotype signature-based high-throughput screening for the discovery of combination immunotherapy compounds. *Sci Adv* 2021;7:eabd7851.
23 Zhang W, Liu HT. MAPK signal pathways in the regulation of cell proliferation in mammalian cells. *Cell Res* 2002;12:9–18.
24 Stutvoet TS, Kol A, de Vries EG, *et al*. MAPK pathway activity plays a key role in PD-L1 expression of lung adenocarcinoma cells. *J Pathol* 2019;249:52–64.
25 Borhani S, Corciulo C, Larranaga-Vera A, *et al*. Adenosine $a_{2a}$ receptor (A2AR) activation triggers akt signaling and enhances

nuclear localization of β-catenin in osteoblasts. *FASEB J* 2019;33:7555–62.
26 Lastwika KJ, Wilson W III, Li QK, *et al*. Control of PD-L1 expression by oncogenic activation of the AKT–mtor pathway in non–small cell lung cancer. *Cancer Res* 2016;76:227–38.
27 Jiang X, Zhou J, Giobbie-Hurder A, *et al*. The activation of MAPK in melanoma cells resistant to BRAF inhibition promotes PD-L1 expression that is reversible by MEK and PI3K inhibition. *Clin Cancer Res* 2013;19:598–609.
28 Bowyer S, Lee R, Fusi A, *et al*. Dabrafenib and its use in the treatment of metastatic melanoma. *Melanoma Manag* 2015;2:199–208.
29 Coelho MA, de Carné Trécesson S, Rana S, *et al*. Oncogenic ras signaling promotes tumor immunoresistance by stabilizing PD-L1 mrna. *Immunity* 2017;47:1083–99.
30 Oh D-Y, Algazi A, Capdevila J, *et al*. Efficacy and safety of pembrolizumab monotherapy in patients with advanced thyroid cancer in the phase 2 KEYNOTE-158 study. *Cancer* 2023;129:1195–204.
31 Zhang M, Gu J, Wang W, *et al*. Combined expression of the BRAFV600E mutation and PD-L1 in early papillary thyroid carcinoma and its relationship with clinicopathological features and recurrence—a retrospective cohort study. *Gland Surg* 2022;11:1908–23.
32 Tuccilli C, Baldini E, Sorrenti S, *et al*. CTLA-4 and PD-1 ligand gene expression in epithelial thyroid cancers. *Int J Endocrinol* 2018;2018:1742951.
33 Means C, Clayburgh DR, Maloney L, *et al*. Tumor immune microenvironment characteristics of papillary thyroid carcinoma are associated with histopathological aggressiveness and BRAF mutation status. *Head & Neck* 2019;41:2636–46.
34 Xie Z, Li X, He Y, *et al*. Immune cell confrontation in the papillary thyroid carcinoma microenvironment. *Front Endocrinol* 2020;11:570604.
35 Veatch JR, Lee SM, Fitzgibbon M, *et al*. Tumor-infiltrating BRAFV600E-specific CD4+ T cells correlated with complete clinical response in melanoma. *J Clin Invest* 2018;128:1563–8.
36 Marabelle A, Fakih M, Lopez J, *et al*. Association of tumour mutational burden with outcomes in patients with advanced solid tumours treated with pembrolizumab: prospective biomarker analysis of the multicohort, open-label, phase 2 KEYNOTE-158 study. *Lancet Oncol* 2020;21:1353–65.
37 Chen S, Wainwright DA, Wu JD, *et al*. CD73: an emerging checkpoint for cancer immunotherapy. *Immunotherapy (Los Angel)* 2019;11:983–97.
38 Jeong YM, Cho H, Kim TM, *et al*. CD73 overexpression promotes progression and recurrence of papillary thyroid carcinoma. *Cancers (Basel)* 2020;12:3042.
39 Huang Z, Pang X, Zhong T, *et al*. Abstract 5526: AK131, an anti-PD1/CD73 bispecific antibody for cancer immune therapy. *Cancer Res* 2022;82:5526.
40 Menzies AM, Long GV, Murali R. Dabrafenib and its potential for the treatment of metastatic melanoma. *Drug Des Devel Ther* 2012;6:391–405.
41 Phadke M, Remsing Rix LL, Smalley I, *et al*. Dabrafenib inhibits the growth of BRAF-WT cancers through CDK16 and NEK9 inhibition. *Mol Oncol* 2018;12:74–88.
42 Danysh BP, Rieger EY, Sinha DK, *et al*. Long-term vemurafenib treatment drives inhibitor resistance through a spontaneous KRAS G12D mutation in a BRAF V600E papillary thyroid carcinoma model. *Oncotarget* 2016;7:30907–23.
43 Dong L, Lv H, Li W, *et al*. Co-expression of PD-L1 and p-AKT is associated with poor prognosis in diffuse large B-cell lymphoma via PD-1/PD-L1 axis activating intracellular AKT/mtor pathway in tumor cells. *Oncotarget* 2016;7:33350–62.
44 Li C-W, Lim S-O, Xia W, *et al*. Glycosylation and stabilization of programmed death ligand-1 suppresses T-cell activity. *Nat Commun* 2016;7:12632.
45 Robert C, Grob JJ, Stroyakovskiy D, *et al*. Five-year outcomes with dabrafenib plus trametinib in metastatic melanoma. *N Engl J Med* 2019;381:626–36.
46 Planchard D, Besse B, Groen HJM, *et al*. Dabrafenib plus trametinib in patients with previously treated brafv600e-mutant metastatic non-small cell lung cancer: an open-label, multicentre phase 2 trial. *Lancet Oncol* 2016;17:984–93.
47 Subbiah V, Kreitman RJ, Wainberg ZA, *et al*. Dabrafenib and trametinib treatment in patients with locally advanced or metastatic BRAF V600-mutant anaplastic thyroid cancer. *J Clin Oncol* 2018;36:7–13.
48 Gutzmer R, Stroyakovskiy D, Gogas H, *et al*. Atezolizumab, vemurafenib, and cobimetinib as first-line treatment for unresectable advanced $BRAF^{V600}$ mutation-positive melanoma (imspire150): primary analysis of the randomised, double-blind, placebo-controlled, phase 3 trial. *Lancet* 2020;395:1835–44.
49 Nathan P, Grob JJ, Dummer R, *et al*. 819P efficacy of dabrafenib (D) trametinib (T) plus spartalizumab (S) by baseline site of metastases in patients (pts) with previously untreated BRAF V600-mutant unresectable or metastatic melanoma: post hoc analysis of phase III COMBI-i trial. *Ann Oncol* 2022;33:S921–2.
50 Welti M, Dimitriou F, Gutzmer R, *et al*. Triple combination of immune checkpoint inhibitors and BRAF/MEK inhibitors in *BRAF*v600 melanoma: current status and future perspectives. *Cancers (Basel)* 2022;14:5489.
51 Haas L, Elewaut A, Gerard CL, *et al*. Acquired resistance to anti-MAPK targeted therapy confers an immune-evasive tumor microenvironment and cross-resistance to immunotherapy in melanoma. *Nat Cancer* 2021;2:693–708.
52 Puzanov I, Ribas A, Robert C, *et al*. Association of BRAF V600E/K mutation status and prior BRAF/MEK inhibition with pembrolizumab outcomes in advanced melanoma: pooled analysis of 3 clinical trials. *JAMA Oncol* 2020;6:1256–64.
53 Atkins MB, Lee SJ, Chmielowski B, *et al*. Combination dabrafenib and trametinib versus combination nivolumab and ipilimumab for patients with advanced *BRAF*-mutant melanoma: the dreamseq trial-ECOG-ACRIN EA6134. *J Clin Oncol* 2023;41:186–97.
54 Ascierto PA, Mandalà M, Ferrucci PF, *et al*. sequencing of ipilimumab plus nivolumab and encorafenib plus binimetinib for untreated*BRAF*-mutated metastatic melanoma (SECOMBIT): a randomized, Three-Arm, Open-Label Phase II trial. *JCO* 2023;41:212–21.
55 Gu Z, Eils R, Schlesner M. Complex heatmaps reveal patterns and correlations in multidimensional genomic data. *Bioinformatics* 2016;32:2847–9.
56 Wang S, Xiong Y, Zhao L, *et al*. UCSCXenaShiny: an R/CRAN package for interactive analysis of UCSC Xena data. *Bioinformatics* 2022;38:527–9.
57 Wickham H. Ggplot2. In: *ggplot2: Elegant Graphics for Data Analysis*. Cham: Springer-Verlag New York, 2016. Available: http://link.springer.com/10.1007/978-3-319-24277-4
58 Mohanty A, Nam A, Srivastava S, *et al*. Acquired resistance to KRAS G12C small-molecule inhibitors via genetic/nongenetic mechanisms in lung cancer. *Sci Adv* 2023;9:eade3816.